Supporting Online Material:

Materials and Methods
SOM text
Figs. S1 and S2
Tables S1 and S2
References

Materials and Methods

Satellite datasets

We used new Visible and Infrared Spectrometer (VIRS) (*1*) and Along Tracking Scanning Radiometer (ATSR) (*2*) satellite data for the timing and location of fires. In the tropics, we used MODerate resolution Imaging Spectroradiometer (MODIS) (*3*) data from the Aqua and Terra satellites to calibrate burned area as a function of detected fires. VIRS data were available for the 38ºN - 38ºS region and started in January 1998, ATSR data were available from the middle of 1996 and had global coverage. We developed a relationship between 'fire counts' (VIRS) and burned area (MODIS) when the two sensors overlapped in 2001. For this fire count to burned area relation, we calculated burned area in 16 MODIS 'tiles', each 10˚ x 10˚. These tiles were located in South America (1), North Africa (1), South Africa (8), and Australia (6) and the relation was constructed in the same fashion as described in *(14)*. This relationship was then used over the full VIRS period (January 1998 - December 2001). To extend our study period back through January of 1997, we developed a separate relation between ATSR and VIRS for each grid cell using the time window when both ATSR and TRMM overlapped (1998-2001). In the extratropics, ATSR fire counts were related to burned area using a single scalar value for all regions north of 38°N. This scaling factor was constructed so that mean burned area over the 1997-2001 period in the biogeochemical model was the same as that derived from a combination of country-level fire statistics and AVHRR-derived burned area estimates in the Russian Far East (*4, 5*). Multi-year analyses of fire emissions using satellite observations have previously been reported (*6-9*) and show large interannual variability. In addition to the satellite data used for fire location and extent, we used the Advanced Very High Resolution Radiometer (AVHRR) satellite for measurements of the fraction of absorbed photosynthetically active radiation (FPAR) by plant canopies (*10, 11*), which is the main driver of net primary production (and thus fuel loads) in our biogeochemical model.

Forward biogeochemical model of fire emissions

The model used in this study to determine fuel loads is based on the Carnegie – Ames – Stanford – Approach (CASA) biogeochemical model (*12*) which was developed to simulate the terrestrial biosphere on seasonal to decadal timescales. We added a fire module that used burned area to calculate what fraction of a grid cell was subject to a fire. Of this fraction, only part of the biomass was actually combusted, depending on the fire induced mortality rate of living biomass and on combustion completeness. We

calculated burned area using relationships between TRMM and ATSR fire counts and MODIS derived burned area that takes into account changes in vegetation density (*13*). Other modifications to the model included herbivory and fuelwood consumption, which simulated fuel loads that were in better agreement with literature values. This is described in detail in a previous paper (*14*). In this study we used an updated and extended set of burned area measurements to calibrate the fire counts, which resulted in higher burned area values and thus higher emissions than those that were previously reported using CASA (*14*). Another important modification in our model concerns the representation of fire induced mortality rates of woody living biomass. Mortality rates were related to fractional tree cover as previously reported (*14*), but the actual shape of the relation changed so that the rates are low (1%) in all grasslands and savanna biomes, and are higher (60%) in forest biomes. The relation between tree mortality (M_w) and fractional tree cover is given below:

$$M_w = 0.01 + 0.59 / (1 + e^{((60 - \% \text{ treecover}) / 4)}) \quad (1)$$

We used climate data (*15*) and accounted for interannual variability in precipitation and temperature using a combination of satellite and station data for precipitation (*16*), and station data for temperature (*17*). Key modeling details included a Net Primary Production (NPP) module based on satellite derived FPAR, solar radiation, and light use efficiency scaled to moisture and temperature conditions. NPP is delivered to living biomass pools (fine roots, stems, and leaves) using fractional tree cover density maps (*18*) to capture carbon dynamics in biomes that fall between closed canopy forests and open grasslands. Depending on biomass turnover time and satellite-derived leaf shedding, the carbon stored in the living biomass pools is delivered to litter pools where soil microbes, fire, fuelwood collection, and herbivory compete for the available carbon. Fire and herbivory also compete for the living biomass pools. Recent changes to the model as described in (*14*) allowed for simulations of global, interannual fire activity and include using burned area in northern regions from country derived statistics and AVHRR satellite data. The model was allowed to reach steady state using mean values of the 1997–2001 data and after spinning up we ran the model for the study period on a monthly, 1º × 1º resolution, allowing for interannual variability in fuel loads caused by changing climate conditions. The increased burned area in forested regions where fuels accumulated over longer periods is the main reason for the observed interannual variability in emissions.

The total carbon flux predicted by our forward biogeochemical model was partitioned into CO_2, CO, and CH_4 fluxes using emissions factors reported for savanna and grassland, tropical forest, and extratropical forests (*19*) and estimated in each 1º×1º according to a map of biomes (*20*). We assumed that the carbon content of dry matter was 45% to calculate the CO_2, CO, and CH_4 emissions from the reported emission factors (*19*).

Chemical Transport Model (CTM)

The forward atmospheric model simulations were performed using the GEOS-CHEM CTM (*21*) at a 4° x 5° horizontal resolution and with 30 vertical levels. The model was driven using meteorological fields from NASA/DAO Data Assimilation

System (DAS) for the year 2000. Our reason for the choice of the specific meteorological dataset is based on the lack of availability of a consistent, multi-year meteorological dataset for the 1997-2001 period from the DAS owing to changes in the underlying general circulation model and the meteorological data used as inputs.

In the atmospheric model, we carried separate tracers of CO_2, CO, and CH_4 for each of the regions listed in Table 1 (a total of 21 tracers). Monthly OH fields were taken from a prior atmospheric simulation (*21*). A global scaling factor of 0.8 is applied to the OH fields for consistency with the estimated lifetime of methyl chloroform against the tropospheric OH sink (*22*). The model calculations were spun up for a period of 3 years during which time we prescribed mean (1997-2001) monthly emissions derived from our biogeochemical model. The model was then integrated for 1 year using emissions from the year 2000 as a proxy for the low fire year of 1996, and then integrated for 5 years from 1997-2001 using monthly emissions from the forward biogeochemical model.

Inversion Formulation

In the inversion procedure we used monthly mean CO data from the National Oceanic and Atmospheric Administration Climate Monitoring & Diagnostics Laboratory (NOAA/CMDL) (http://www.cmdl.noaa.gov/ccg/). Since our inversion operated on CO anomalies, we only included stations that allowed us to construct a mean seasonal cycle over the 1997-2001 period. All of the following 56 stations met this criteria and as a minimum had at least 30 monthly mean observations during the 60 month study period from January 1997 through December 2001: ALT, ZEP, BRW, STM, ICE, CBA, BAL, MHD, SHM, HUN, LEF, KZD, BSC, UUM, KZM, NWR, UTA, AZR, TAP, WLG, BME, BMW, WIS, POCN30, MID, IZO, POCN25, KEY, ASK, POCN20, KUM, MLO, POCN15, RPB, GMI, POCN10, POCN05, POC000, SEY, POCS05, ASC, POCS10, SMO, POCS15, POCS20, POCS25, EIC, POCS30, POCS35, CGO, CRZ, TDF, PSA, SYO, HBA, and SPO.

As a first step, we removed the mean seasonal cycle from the data at each station. We then binned this data into 6 latitude zones (90°N-60°N, 60°N-30°N, 30°N-0°N, 0°S-30°S, 30°S-60°S, and 60°S-90°S) and constructed a mean time series of the CO anomaly for each zone. These observed anomalies were used to construct a data vector that consisted of 360 values (6 latitude zones each containing 60 monthly mean observations). The basis regions for the inversion consisted of the seven regions listed in Table 1. In each basis region, the monthly pattern of CO emissions was specified over the 1997-2001 period from our forward biogeochemical model and used to drive the atmospheric model (see CTM description above). Model simulated CO time series taken from the model grid cells containing the CMDL stations were processed using the exact same procedure described above for the CMDL station data. The G matrix (*23*) had dimensions of 7 columns (one for each basis region) and 360 rows (corresponding to 6 latitude zones, and 60 monthly mean model-derived CO anomalies within each zone). We assumed that the measurement error associated with CO observations was 5 ppb at all stations. The scalars obtained from the least squares inversion (Table 1), that minimized the difference between model-predicted and observed CO concentration anomalies at remote flask stations over the 1997-2001 period, can be thought of as adjustments to our regional forward model emissions estimates. Since we did not

impose any non-negativity constraints in the inversion, that the resulting scalars we obtained were positive makes physical sense and is one of several lines of evidence that suggests our inverse problem was well posed.

We should note that, because we focused on CO concentration anomalies, our CO inversion did not provide meaningful constraints on the magnitude of mean absolute annual emissions; for these we relied on our forward biogeochemical model that had uncertainties caused by the satellite data and our representations of mortality, combustion completeness, and fuel loads. Previous inversion studies have explored biomass burning contributions to mean seasonal and latitudinal patterns of atmospheric CO (*24*), and new observations from the Measurements Of Pollution In The Troposphere (MOPITT) instrument should significantly improve the mean seasonal dynamics of emissions inventories from fire in tropical regions.

Sensitivity of Results to the Inversion Problem Formulation

We also conducted a separate formulation of the inversion in which we did not aggregate the observations or model concentrations into 6 latitudinal zones. Instead, observations from each station were appended to one another as rows in our G matrix. The number of basis regions remained the same (7), and so the size of the G matrix was 7 columns and 3033 rows (representing 56 stations each with a mean of 53 monthly mean observations at each station during the 97-01 period). Again, measurement errors were assumed to be uniform at 5 ppb for each monthly mean observation.

From this formulation we obtained a similar, but not identical, set of scalars. Specifically, we obtained coefficients of 1.68 for Central and northern South America, 0.73 for southern South America, 0.36 for Africa north of the equator, 0.33 for Africa south of the equator, 3.25 for Southeast Asia, 1.42 for boreal forests, and -1.20 for 'Other' regions. For Southeast Asia, Central America and northern South America, and boreal regions, somewhat lower CO emissions were required for the least squares solution than for the primary inversion formulation reported in Table 1. For southern South America, the scalar remained about the same (0.73 vs. 0.69 reported in Table 1). In Africa, the scalar dropped north of the equator but increased south of the equator. 'Other' regions switched from a positive value (1.13) to a negative value of equal magnitude (-1.15). While Africa and 'Other' regions showed a higher sensitivity to the inversion formulation, these were regions that contributed only minimally to the observed variability in fluxes over this period (Table 1 and Table S2).

This second inversion formulation suggests that our results are somewhat sensitive to the design of the inversion problem, but does not significantly alter our conclusion that Central America and northern South America, boreal forests, and southern South America accounted for a significant fraction of the trace gas variability during the extreme 1997-1998 El Niño event. The global emissions anomaly during the El Niño period using this inversion approach was 2.0 Pg C. This is slightly lower than that predicted by our primary inversion approach reported in the text and in Table 1. The partitioning of this anomaly across Southeast Asia, Central and northern South America, boreal regions, and southern South America (54%, 20%, 10%, and 12%, respectively) was similar to that reported in the text, but required even greater relative contributions from source regions other than Southeast Asia.

Supporting Online Material text

Partitioning fire emissions anomalies within continental regions

We partitioned the inversion-derived continental emissions anomalies reported in Table 1 among countries by making the following two assumptions. First, we assumed that the relative spatial distribution of fire emissions from the forward biogeochemical model was correct. Second, we assumed that the inversion-derived scalar operated linearly on each 1˚ x 1˚ model grid cell within each of the continental regions.

Following these assumptions, within Southeast Asia, the fire emissions anomaly during the El Niño period (1.34 ± 0.67 Pg C) was distributed across Indonesia (52%), Papua New Guinea (13%), and Malaysia (8%) with smaller contributions from neighboring countries according to our satellite-driven biogeochemical model. Within Indonesia, most of the emissions anomaly originated in Kalimantan (63%), Sumatra (18%), and Irian Jaya (13%). Within Central America and northern South America, the fire emissions anomaly during the El Niño period (0.45 ± 0.31 Pg C) occurred mostly within Mexico (54%), Venezuela (17%), and Guatemala (7%). In boreal regions, the inversion estimate of the carbon emissions anomaly from fire during 1998 was 0.32 ± 0.17 Pg C. This anomaly was distributed mostly within the Russian Far East (71%) and Canada (28%). An independent 'bottom up' approach based on burned area statistics reported by individual countries in the northern extra tropics and a separate emissions model (that accounted for peat burning) achieved a similar east-west partitioning (*25*).

Sources of uncertainty

There are three primary reasons why the global carbon emissions anomaly from fires estimated here is likely to represent an upper bound. First, the emission factors and forward biogeochemical model we used did not explicitly account for peat burning in tropical or boreal forests. Measurements from temperate and boreal regions (*26*) indicates that peat burning, which is mostly emitted during the smoldering stage of a fire, emits 2 to 3 times more products of incomplete combustion such as CO and CH_4 than fires in savannas and forests (*19, 27*). Thus, in terms of explaining the observed atmospheric CO anomalies, less total carbon emissions are required when CO emissions factors are large. Aircraft measurements near the 1997 Indonesian fires show very low NO_x (emitted mostly during a flaming stage of a fire) to CO (emitted mostly during the smoldering stage of a fire) ratios, provide regional–scale evidence for smoldering combustion (*28*), and support ground-based measurements that implicate peat burning as the primary source of emissions (*29*). However, other aircraft measurements (*30*) report $CO:CO_2$ ratios near Indonesia of 0.089 that were similar to (or even lower than) the values used here (Table 1).

Second, the observed space-time pattern of CO anomalies (Fig. 2) caused the inversion to attribute a significant part of the trace gas anomalies in the northern hemisphere to boreal fires. Per unit of emitted trace gas, emissions from the boreal zone have a larger impact on atmospheric concentrations near the surface than emissions from the tropics because of properties of atmospheric mixing. Specifically, poleward transport of air from the tropics tends to occur aloft in the mid or upper troposphere, where CO from tropical fires would have been diluted and partially destroyed by oxidation with OH before returning to the surface. By contrast, the return flow to the

tropics tends to occur near the surface, which would have brought CO anomalies from boreal fires in contact with multiple surface observation stations in a shorter period of time, with less of a chance for dilution or oxidation. For this reason, the sum of global emissions anomalies reported here is somewhat lower than previous modeling estimates that assumed emissions occurred in a well-mixed atmosphere (*31*).

Third, in our atmospheric chemistry model runs, we used climatological monthly mean OH concentrations (*21*). Given the large perturbations to CO and CH_4 in some regions of the atmosphere, it is likely that the high fire emissions in 1997-1998 caused a decrease in OH and a corresponding increase in the lifetimes of CO and CH_4 (*32*). In terms of the inversion, accounting for these non-linear feedbacks would require smaller CO emissions anomalies from source regions.

If we were to assume the extreme case that all of the emissions anomaly in Southeast Asia was caused by peat burning, and that therefore the emission factor of CO would double (*27*), then the amount of carbon required to explain the CO anomaly in Southeast Asia would decrease by 50%, and the global total carbon anomaly would decrease to 1.45 ± 0.59, which still would explain about 45% of the observed CO_2 growth rate anomaly. As described above, satellite evidence for increased fire emissions across Indonesia, Malaysia, and Papua New Guinea within Southeast Asia during 1997 suggests that a 100% peat land scenario is unlikely. Nevertheless, the uncertainties arising from a lack of representing peat lands and uncertainties of burned area estimates in closed canopy forests are probably the two most important reasons for the discrepancies between our forward and inverse modeling estimates for Southeast Asia.

Other terrestrial mechanisms

Climate responses of terrestrial processes other than fire have been proposed to explain interannual variability in the atmospheric CO_2 growth rate. These include drought inhibition of photosynthesis (*33-36*), warm temperature stimulation of ecosystem respiration (*37-39*), a combination of both (*40-42*), or changes in cloud induced light limitation on photosynthesis (*43, 44*). In this study we did not address the potential impacts of climate induced variability on autotrophic respiration (*37, 39*) or diffuse light effects on photosynthesis (*43, 44*). The predicted magnitude of the contributions of fire emissions to CO_2 anomalies reported here is independent of these issues because it was derived from the atmospheric CO signal, with CASA providing only the timing and spatial distribution of fire emissions within each region. It may be that the variations in photosynthesis and respiration during this period were much larger but cancelled each other out (e.g. photosynthesis and respiration were both stimulated or inhibited). Our study indicates that attributing the entire observed CO_2 signal to photosynthesis-respiration balance while neglecting variability of fire emissions may result in a misinterpretation of the degree to which land physiological processes respond to climate variability.

Supporting Figures

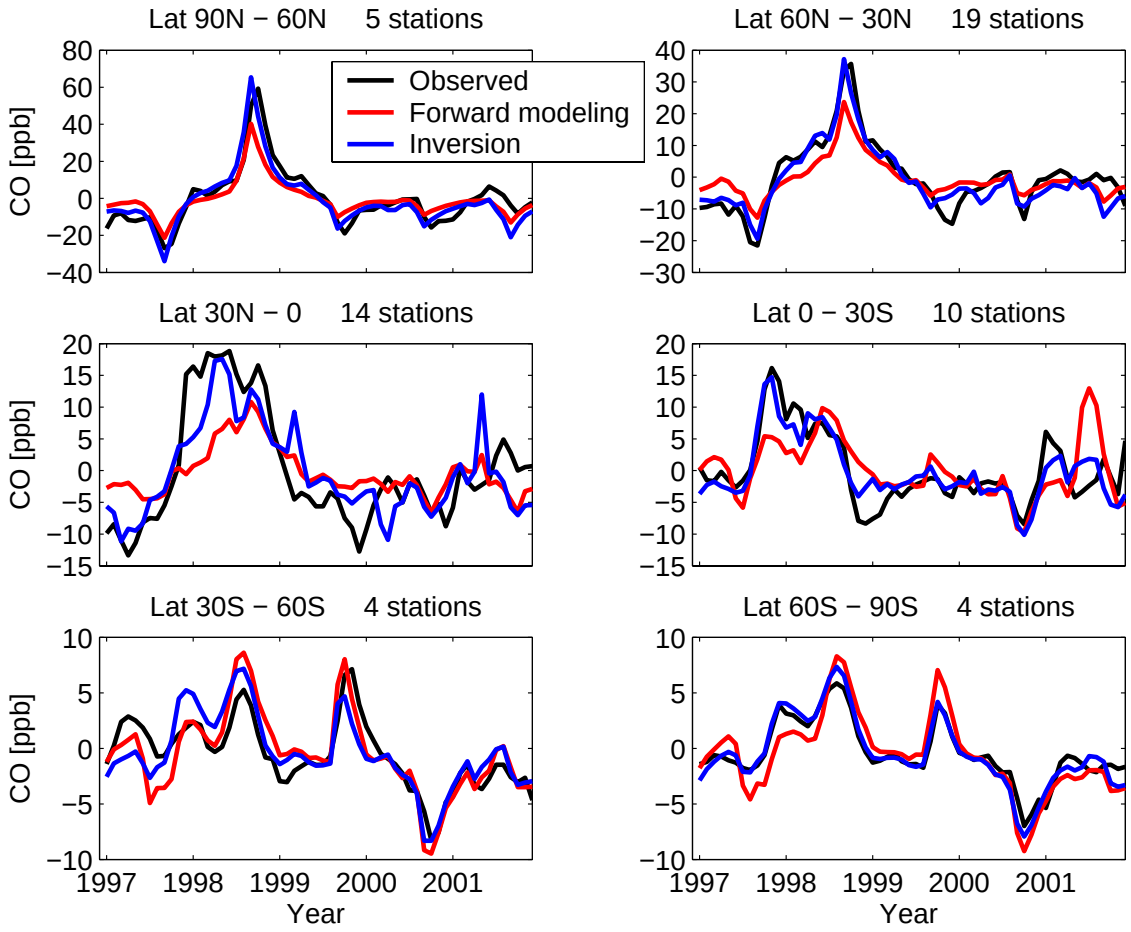

Fig. S1. Observed CO concentration anomalies for 6 different latitude zones, along with fire contributions obtained from the forward model and from the atmospheric inversion based on NOAA/CMDL flask CO data. The correlation (r) between the inversion and observations was higher in 5 out of 6 latitude regions than the correlation between the forward model and observations: 90°N-60°N 0.93 vs. 0.92, 60°N-30°N 0.95 vs. 0.93, 30°N-equator 0.87 vs. 0.83, equator-30°S 0.85 vs. 0.64, 30°S-60°S 0.75 vs. 0.77, 60°S-90°S 0.92 vs. 0.88.

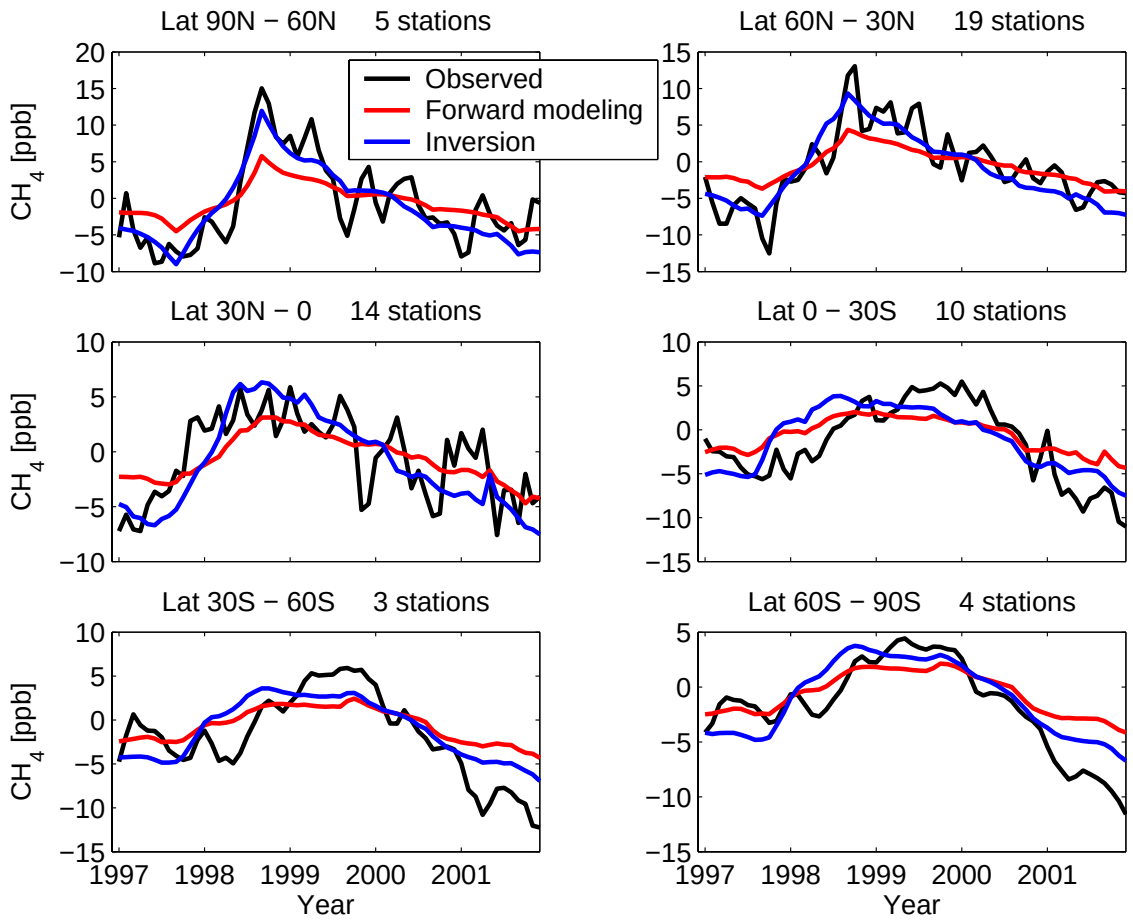

Fig. S2. Observed CH_4 concentration anomalies for 6 different latitude zones, along with fire contributions obtained from the forward model and from the atmospheric inversion based on NOAA/CMDL flask CO data and on published CO and CH_4 emission factors. In the northern hemisphere, fire emissions accounted for almost all of the observed CH_4 concentration anomalies during the study period, with dominant and roughly equal contributions from boreal regions and Southeast Asia (~ 40% each), and a minor contribution from Central America (~10%). In the southern hemisphere, the fire component was greater than the observed concentration anomalies during early 1998. This offset may have been caused by uncertainties associated with the CO inversion or by uncertainties from emission factors, although these are expected to be small since emissions of CO and CH_4 both occur in the smoldering phases of combustion and usually co-vary. The offset is also consistent with drought stress driving down CH_4 emissions in tropical wetlands at the same time that CH_4 emissions from fires were increasing.

Supporting Tables

Table S1. CO anomalies and 95% confidence limits (Tg CO) from fires during the 1997-1998 El Niño and the 1997-2001 period derived from the inversion.

	Timeframe of CO anomalies					
Region of Fire Emissions	1997-1998 El Niño	1997	1998	1999	2000	2001
Central + northern S-America	90 ± 40	-19 ± 9	81 ± 36	-31 ± 14	-22 ± 10	-10 ± 4
Southern S-America	48 ± 23	21 ± 10	22 ± 11	11 ± 5	-39 ± 19	-16 ± 8
Northern Africa	-21 ± 21	10 ± 10	12 ± 12	-9 ± 9	10 ± 10	-23 ± 23
Southern Africa	6 ± 17	-4 ± 13	6 ± 19	-1 ± 4	-1 ± 2	0 ± 0
Southeast Asia	300 ± 62	159 ± 33	66 ± 14	-43 ± 9	-128 ± 27	-53 ± 11
Boreal (regions north of 38ºN)	57 ± 4	-30 ± 2	76 ± 6	-18 ± 1	-5 ± 0	-22 ± 2
Other	-5 ± 8	-2 ± 3	-11 ± 16	7 ± 10	0 ± 1	6 ± 9
Global	474 ± 82	134 ± 39	253 ± 49	-85 ± 22	-185 ± 36	-118 ± 29

Table S2. Percent contribution of regional fire emissions to monthly variability in atmospheric CO anomalies during 1997-2001

	Latitude zone of atmospheric CO anomalies						
Region of Fire Emissions	90°N to 60°N	60°N to 30°N	30°N to 0°N	0°S to 30°S	30°S to 60°S	60°S to 90°S	Global
Central America + northern S-America	0.3	3.4	13.7	6.5	6.4	6.3	7.3
southern S-America	0.0	0.1	0.8	8.9	33.8	40.1	11.3
Africa north of equator	0.1	0.3	1.7	4.5	2.3	2.3	2.2
Africa south of equator	0.0	0.0	0.0	0.4	0.8	0.7	0.3
Southeast Asia	4.8	15.2	57.5	78.6	51.3	47.6	49.7
Regions north of 38ºN	94.7	80.9	26.2	0.4	0.2	0.2	27.8
Other	0.0	0.1	0.0	0.8	5.2	2.8	1.4

References

1. L. Giglio, J. D. Kendall, C. J. Tucker, *Int. J. Remote Sens.* **21**, 203 (2000).
2. O. Arino, J-M. Rosaz, P. Goloub, *Earth Obs. Quart.* **64**, 1 (1999).
3. C. O. Justice *et al.*, *Remote Sens. Environment* **83**, 244 (2002).
4. E. S. Kasischke, D. Williams, D. Barry, *Int. J. Wildland Fire* **11**, 131 (2002).
5. B. J. Stocks *et al.*, *J. Geophys. Res.* **108**, 8149 (2002).
6. P. M. Barbosa, D. Stroppiana, J. M. Gregoire, J. M. C. Pereira, *Global Biogeochem. Cycles* **13**, 933 (1999).
7. B. N. Duncan, R. V. Martin, A. C. Staudt, R. Yevich, J. A. Logan, *J. Geophys. Res.* **108**, 4100 (2003).
8. B. D. Amiro *et al.*, *Can. J. For. Res.* **31**, 512 (2001).
9. M. G. Schultz, *Atm. Chem. Phys.* **2**, 387 (2002).
10. S. O. Los, C. Justice, C. J. Tucker, *Int. J. Remote Sens.* **15**, 3493 (1994).
11. D. A. Slayback, J. E. Pinzon, S. O. Los, C. J. Tucker, *Global Change Biol.* **9**, 1 (2003).
12. C. S. Potter *et al.*, *Global Biogeochem. Cycles* **7**, 811 (1993).
13. R. J. Scholes, J. Kendall, C. O. Justice, *J. Geophys. Res.* **101**, 23667 (1996).
14. G. R. van der Werf, J. T. Randerson, G. J. Collatz, L. Giglio, *Global Change Biol.* **9**, 547 (2003).
15. R. Leemans, W. P. Cramer, "The IIASA database for mean monthly values of temperature, precipitation and cloudiness of a global terrestrial grid" (Int. Inst. Appl. Sys. Anal, 1990).
16. R. F. Adler *et al.*, *J. Hydrometeorology* (2003).
17. J. Hansen, R. Ruedy, J. Glascoe, M. Sato, *J. Geophys. Res.* **104**, 30997 (1999).
18. R. S. DeFries, J. R. G. Townshend, M. C. Hansen, *J. Geophys. Res.* **104**, 16911 (1999).
19. M. O. Andreae, P. Merlet, *Global Biogeochem. Cycles* **15**, 955 (2001).
20. R. DeFries, M. Hansen, J. Townshend, *Remote Sens. Environment* **54**, 209 (1995).
21. I. Bey *et al.*, *J. Geophys. Res.* **106**, 23073 (2001).
22. P. Kasibhatla, A. Arellano, J. A. Logan, P. I. Palmer, P. Novelli, *Geophys. Res. Lett.* **29**, 1900 (2002).
23. W. Menke, *Geophysical Data Analysis: Discrete Inverse Theory* (Academic Press, 1989).
24. P. Bergamaschi, R. Hein, M. Heimann, P. J. Crutzen, *J. Geophys. Res.* **105**, 1909 (2000).
25. E. S. Kasischke, L. P. Bruhwiler, *J. Geophys. Res.* **107**, 8146 (2002).
26. R. J. Yokelson, R. Susott, D. E. Ward, J. Reardon, D. W. T. Griffith, *J. Geophys. Res.* **102**, 18865 (1997).
27. J. S. Levine, *Geophys. Res. Lett.* **26**, 815 (1999).
28. Y. Sawa *et al.*, *Geophys. Res. Lett.* **26**, 1389 (1999).
29. S. E. Page *et al.*, *Nature* **420**, 61 (2002).
30. H. Matsueda, H. Y. Inoue, M. Ishii, Y. Tsutsumi, *J. Geophys. Res.* **104**, 26867 (1999).
31. R. L. Langenfelds *et al.*, *Global Biogeochem. Cycles* **16**, 1048 (2002).

32. P. C. Novelli *et al.*, *J. Geophys. Res.* **108**, 4464 (2003).
33. R. R. Nemani *et al.*, *Science* **300**, 1560 (2003).
34. H. Q. Tian *et al.*, *Nature* **396**, 664 (1998).
35. C. D. Jones, M. Collins, P. M. Cox, S. A. Spall, *J. Clim.* **14**, 4113 (2001).
36. D. Fujita *et al.*, *Tellus* **55**, 530 (2003).
37. J. Kindermann, G. Wurth, G. H. Kohlmaier, F. W. Badeck, *Global Biogeochem. Cycles* **10**, 737 (1996).
38. J. C. Gerard, B. Nemry, L. M. Francois, P. Warnant, *Geophys. Res. Lett.* **26**, 243 (1999).
39. D. A. Clark, S. C. Piper, C. D. Keeling, D. B. Clark, *Proc. Natl. Acad. Sci. U.S.A.* **100**, 5852 (2003).
40. W. Knorr, *Global Ecol. Biogeography* **9**, 225 (2000).
41. K. Schaefer *et al.*, *Global Biogeochem. Cycles* **16**, 1102 (2002).
42. M. K. Cao, S. D. Prince, H. H. Shugart, *Global Biogeochem. Cycles* **16**, 1069 (2002).
43. X. Yang, M. Wang, *Geophys. Res. Lett.* **27**, 1671 (2000).
44. E. A. Graham, S. S. Mulkey, K. Kitajima, N. G. Phillips, S. J. Wright, *Proc. Natl. Acad. Sci. U.S.A.* **100**, 572 (2003).